Electronic Supplementary Information for Two-dimensional ferroelasticity and ferroelastic strain controllable anisotropic transport properties in CuTe monolayer†

Xinkai Ding[a] and Gaoyang Gou*[a,b]

* *To whom correspondence should be addressed: gougaoyang@mail.xjtu.edu.cn*

[a] *Frontier Institute of Science and Technology, and State Key Laboratory for Mechanical Behavior of Materials, Xi'an Jiaotong University, Xi'an 710049, China*

[b] *Collaborative Innovation Center of Quantum Information of Shaanxi Province, Xi'an 710071, China*

The scattering time approximation

For simulations of the Seebeck coefficient and other transport coefficients, we use Boltzmann transport formalism under the constant scattering time (τ) approximation as implemented in the boltztrap2 code. Here, the relaxation time τ can be obtained from fitting the room-temperature conductivity σ by:

$$\tau = \frac{\sigma m^*}{ne^2} \tag{S1}$$

where the e denotes the electron charge, and the n denotes the electron density of the system. For metallic systems, the effective mass m^* can be replaced by the electronic mass m_e. Based on experimentally measured electrical resistivity (ρ), the electrical conductivity (σ) for CuTe single crystal can be obtained by: $\sigma = 1/\rho$.

Table S1 SCAN+rVV10 calculations predicted lattice parameters for 3D CuTe bulk with *Pmmn* symmetry, compared with the experimental results[1].

Lattice parameters	a (Å)	b (Å)	c (Å)
Cal.	3.16	3.96	6.97
Exp.	3.16	4.08	6.93

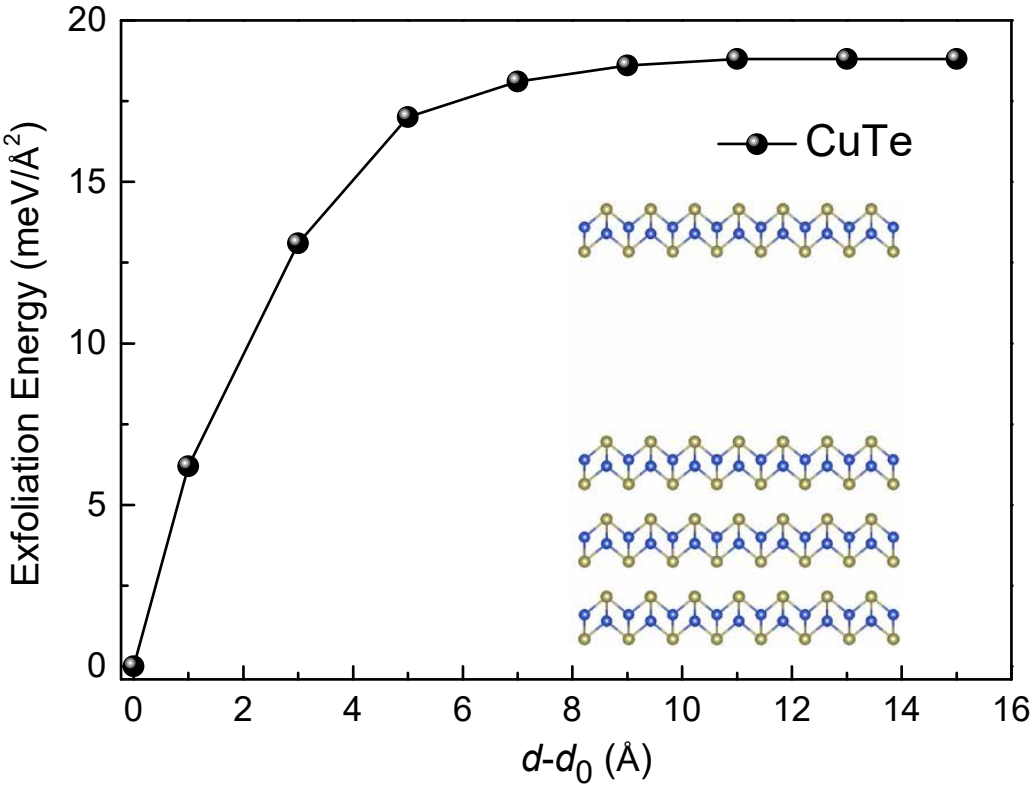

Figure S1 The variation of system energy as a function of interlayer distance when 2D CuTe monolayer is exfoliated from the 3D bulk counterpart.

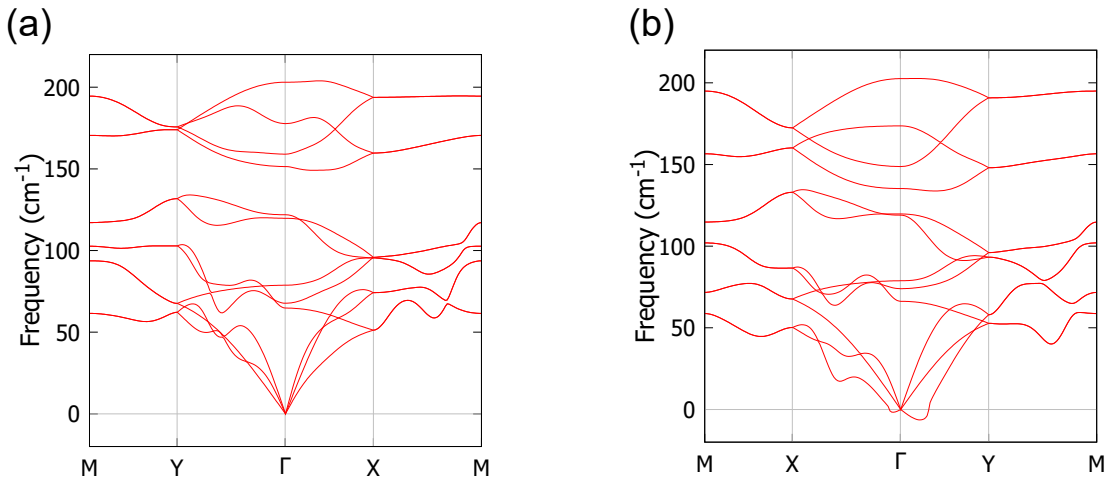

Figure S2 Our simulated phonon spectra of (a) 2D FE CuTe monolayer and (b) 3D CuTe bulk using PHONOPY code[2].

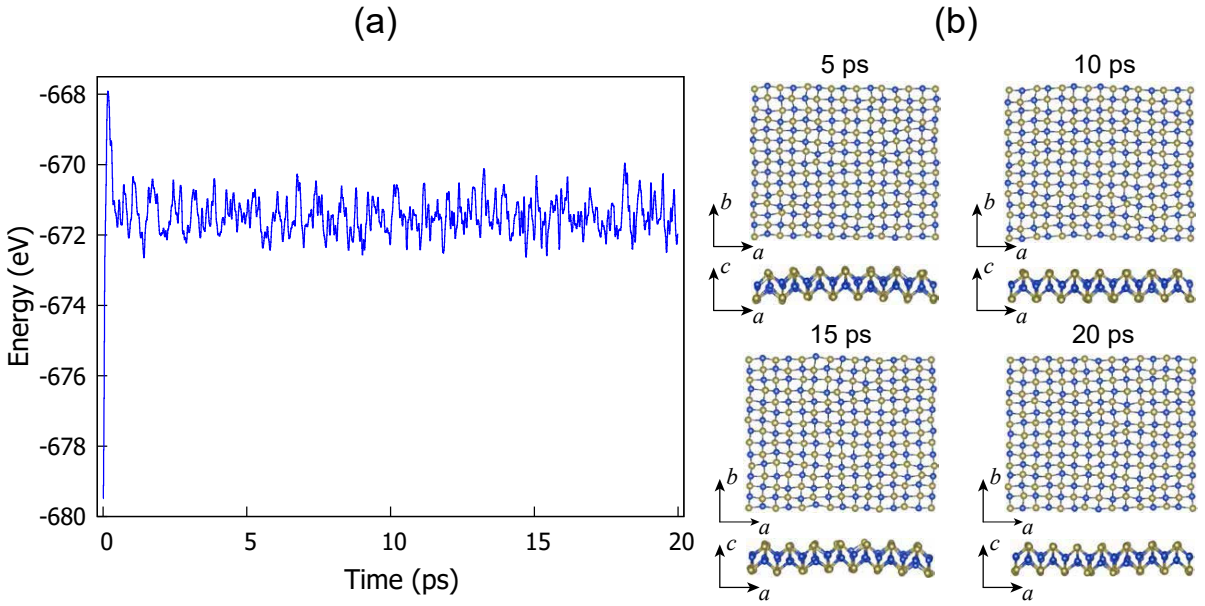

Figure S3 (a) Full time evolution of the total energy for CuTe monolayer composed of 7×7 CuTe primary unit cells, during *ab initio* MD simulations performed at 300 K up to 20 ps. (b) Four CuTe monolayer snapshot structures are extracted from MD simulations when the computational time reaches 5 ps, 10 ps, 15 ps and 20 ps, respectively. Each CuTe monolayer snapshot structure has the orthorhombic planar lattice distortion (normalized lattice parameter $a > b$) and therefore non-zero FE strain, indicating 2D ferroelasticity of CuTe monolayer can persist at the room temperature.

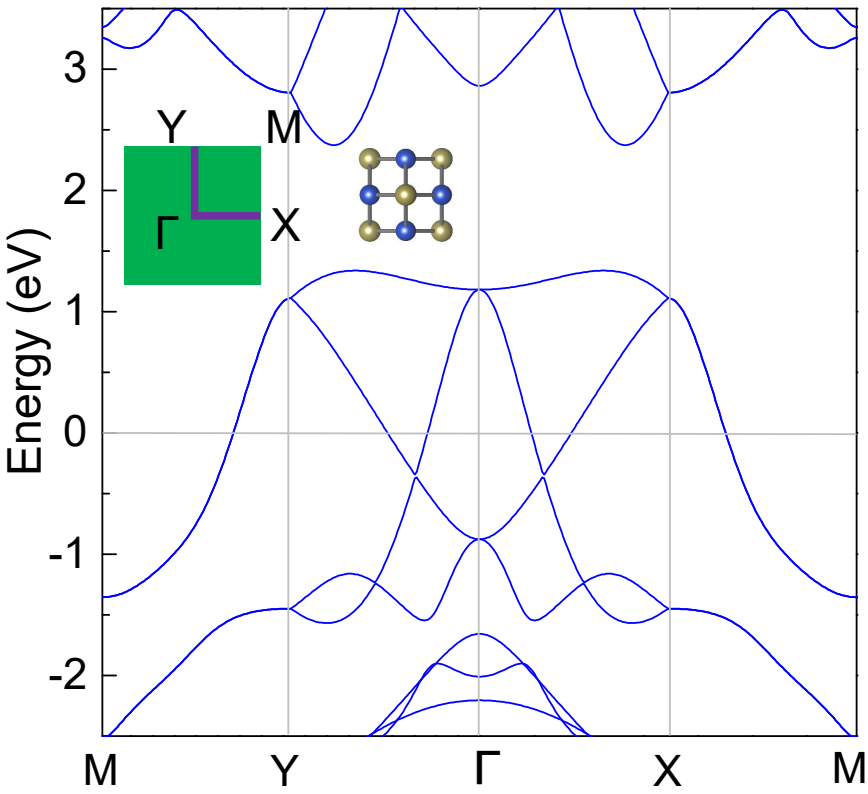

Figure S4 PE phase of CuTe monolayer calculated using SCAN+rVV10 functional with SOC effect included. PE CuTe monolayer has the in-plane isotropic electronic structures: energy bands along both Γ-X and Γ-Y directions are degenerate.

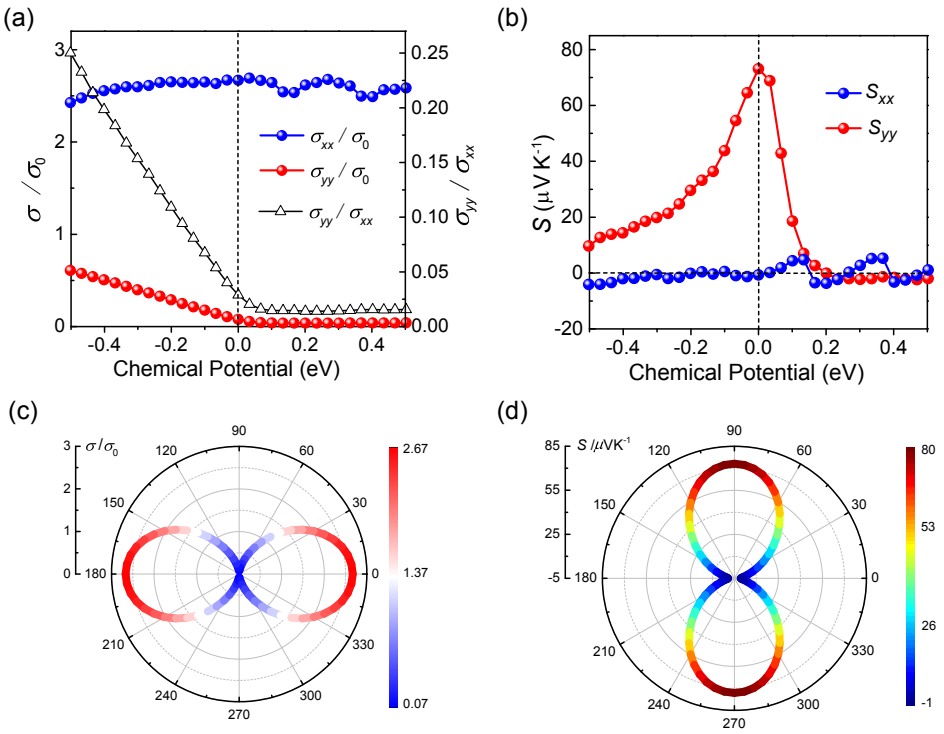

Figure S5 Anisotropic transport properties for FE-II domain variant of CuTe monolayer. (a) Relative electrical conductivity σ/σ_0 and (b) thermopower coefficient S as a function of chemical potential simulated around room temperature. σ_{yy}/σ_{xx} in black color indicates the magnitude of in-planar electrical conductivity anisotropy. The evolution of the simulated (c) electrical conductivity σ/σ_0 and (d) thermopower coefficient S under the zero chemical potential of CuTe monolayer as a function of the angle θ relative to [100] crystallographic direction.

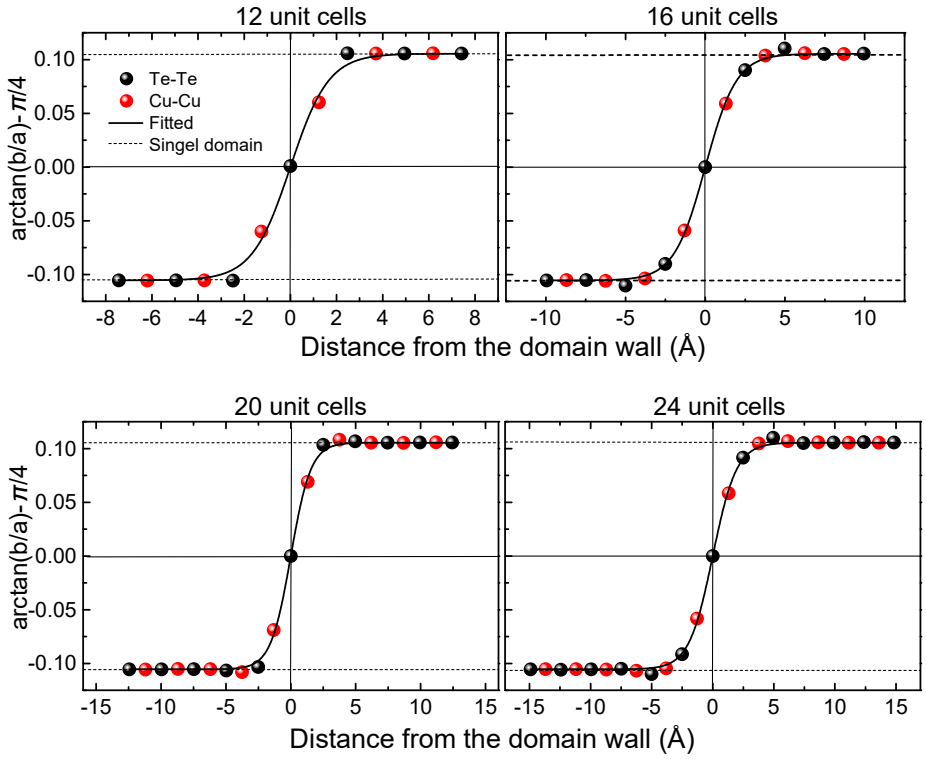

Figure S6 Distribution of FE strain across the domain boundary in all multi-domain configurations, which contain N (N = 12, 16, 20, 24) CuTe unit cells stacking along the direction perpendicular to domain walls.

Table S2 The calculated lattice parameter l_y (Å) along y axis, domain wall energies E_{DW} (meV/Å) and domain wall width $2\xi_{\mathrm{DW}}$ (Å) from the domain-wall configurations containing different number of CuTe unit cells. Domain wall energies are computed as: $E_{\mathrm{DW}} = (E - E_0)/2l_y$, E is the energy of the domain-wall configuration, E_0 is the reference energy of CuTe single FE domain evaluated for the same supercell, the factor 2 means the presence of twin walls in one supercell.

Number of unit cells	12	16	20	24
l_y	5.046	5.050	5.046	5.050
E_{DW}	39.524	35.844	34.236	32.639
$2\xi_{\mathrm{DW}}$	3.313	3.919	3.103	3.900

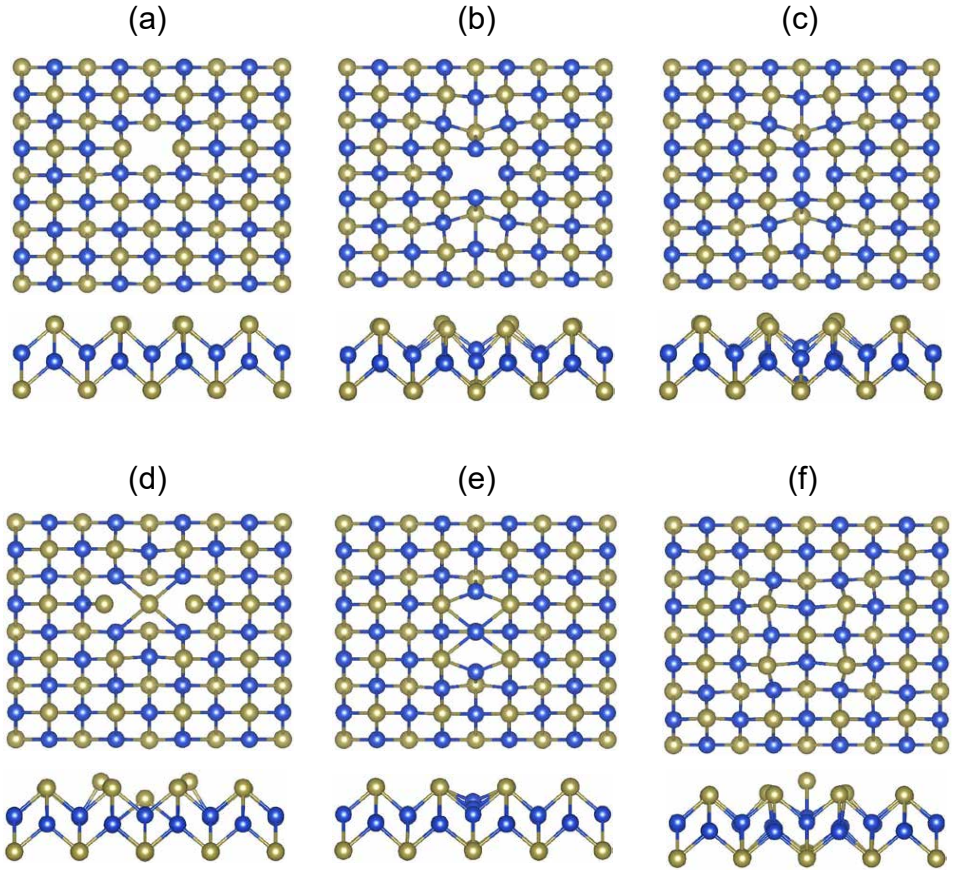

Figure S7 Our optimized crystal structures for defective CuTe monolayer composed of 4×4 CuTe primary unit cells containing a single Cu or Te atom vacancy (V_{Cu}, V_{Te}), antisite defects (incorporation of a single Te/Cu atom into Cu/Te ionic site, Te_{Cu}, Cu_{Te}), Cu, Te interstitial defect (Cu_i, Te_i).Both top and side views for our optimized (a) V_{Cu}, (b) V_{Te}, (c) Te_{Cu}, (d) Cu_{Te}, (e) Cu_i and (f) Te_i defective CuTe monolayer crystal structures are provided.

Figure S7 displays CuTe supercell configuration we constructed to simulate the defective CuTe monolayer, where the formation of a single Cu, Te atom vacancy (V_{Cu}, V_{Te} under Kroger-Vink notation), antisite defect (occupation of Te/Cu ionic site by Cu/Te atom, Cu_{Te}, Te_{Cu}), as well as the incorporation of a single Cu, Te atom at the interstitial site (Cu_i, Te_i) are considered for simulations. After structural optimization, V_{Cu} defect induces the least distortion for CuTe monolayer lattice. In the meanwhile, our calculations also indicate V_{Cu} defect characterizes the smallest defect formation energy under both Cu and Te rich conditions among all defects we simulated (Table S3). V_{Cu} is therefore chosen as the most easily formed point defect where the FE switching kinetcs within the defective CuTe monolayer will be simulated.

Table S3 Our calculated defect formation energies (E_f in eV) for vacancy, antisite and intersitial defects in CuTe monolayer, under both Cu and Te rich conditions. The defect formation energy E_f is defined as: $E_f = E_{defect} - E_{pristine} - n_{\mathrm{Cu}}\mu_{\mathrm{Cu}} - n_{\mathrm{Te}}\mu_{\mathrm{Te}}$, where E_{defect} and $E_{pristine}$ are DFT total energies for the defective and pristine CuTe monolayer evaluated under the same supercell size, $n_{\mathrm{Cu}}(n_{\mathrm{Te}})$ is the number of Cu(Te) atoms exchanged between the defective CuTe monolayer and the atomic reservoir with chemical potential $\mu_{\mathrm{Cu}}(\mu_{\mathrm{Te}})$. Considering the equilibrium condition of CuTe monolayer, μ_{Cu} and μ_{Te} satisfy the relation: $\mu_{\mathrm{Cu}} + \mu_{\mathrm{Te}} = E_{\mathrm{CuTe}}$, where E_{CuTe} is the normalized energy (per Cu-Te pair) of the pristine CuTe monolayer. Under Cu(Te)-rich condition, bulk Cu(Te) can be used as the reservoir for $\mu_{\mathrm{Cu}}(\mu_{\mathrm{Te}})$, respectively.

Configurations	Cu-rich	Te-rich
$\mathrm{V_{Cu}}$	0.393	0.265
$\mathrm{V_{Te}}$	1.337	1.465
$\mathrm{Te_{Cu}}$	1.157	1.414
$\mathrm{Cu_{Te}}$	2.144	1.888
$\mathrm{Cu_i}$	0.619	0.747
$\mathrm{Te_i}$	1.630	1.502

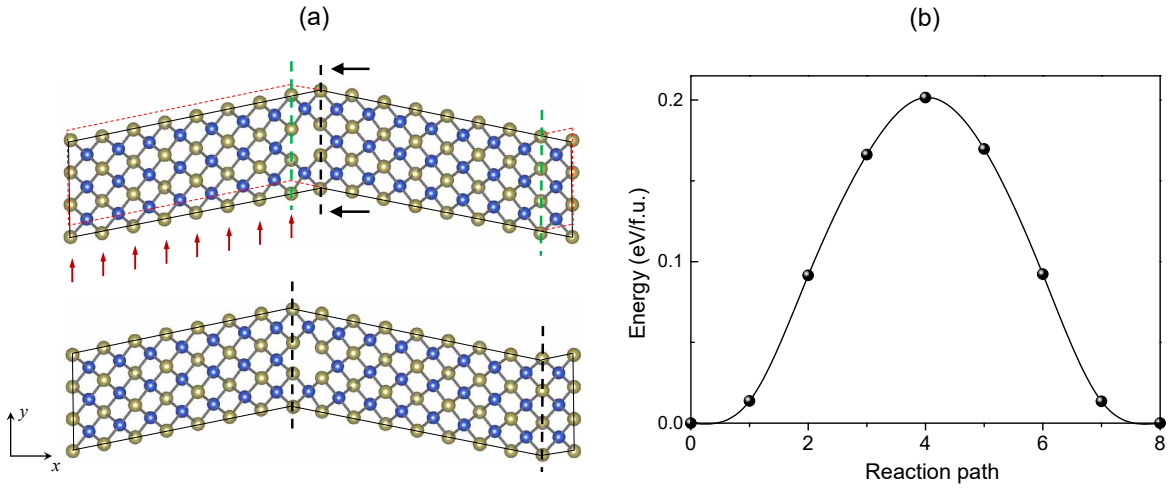

Figure S8 The transformation pathway and energy barrier for domain-wall motion assisted FE switching in the defective CuTe monolayer containing V_{Cu} defect, calculated by the CI-NEB method. (a) Migration of FE domain wall across V_{Cu} defect is achieved by the rigid shift of atomic positions for one FE domain variant (indicated by red arrows). (b) Change of the normalized system energy as a function of reaction path along the transformation pathway. Our simulated energy barrier associated with domain wall motion in the defective CuTe monolayer is one order of magnitude larger than that of the pristine CuTe monolayer.

The transverse effect in two-dimensional materials

Generally, a thermoelectric material will exhibit Seebeck effect, where the temperature gradient ∇T can give arise to the non-zero electric current density $\boldsymbol{j}$, described by:

$$\boldsymbol{j} \propto S \cdot \nabla T \tag{S2}$$

where S is thermopower coefficient. Specifically, for a 2D material with two planar principal x and y axes, S coefficient can be described by a 2×2 tensor matrix. Assuming temperature gradient is applied along the planar x axis ($\frac{\partial T}{\partial x}$), then the generated electric current density is given by:

$$\boldsymbol{j} \propto S \cdot \nabla T = \begin{pmatrix} S_{xx} & 0 \\ 0 & S_{yy} \end{pmatrix} \cdot \begin{pmatrix} \frac{\partial T}{\partial x} \\ 0 \end{pmatrix} = \begin{pmatrix} S_{xx} \cdot \frac{\partial T}{\partial x} \\ 0 \end{pmatrix} \tag{S3}$$

Here, the output electric current density only appears along the principal x axis. Without losing generality, we consider the case where temperature gradient is applied along a direction with the angle θ relative to x axis. Then S tensor matrix adopts the following form:

$$\begin{pmatrix} S'_{xx} & S'_{xy} \\ S'_{yx} & S'_{yy} \end{pmatrix} \tag{S4}$$

where

$$\begin{aligned} S'_{xx} &= S_{xx} \cdot \cos^2\theta + S_{yy} \cdot \sin^2\theta, \\ S'_{yy} &= S_{yy} \cdot \cos^2\theta + S_{xx} \cdot \sin^2\theta, \\ S'_{yx} = S'_{xy} &= \frac{S_{xx} - S_{yy}}{2} \cdot \sin 2\theta = \frac{1}{2}\Delta S \cdot \sin 2\theta. \end{aligned} \tag{S5}$$

As a result, Equation S3 can be reformulated as:

$$\boldsymbol{j} \propto S \cdot \nabla T = \begin{pmatrix} S'_{xx} & S'_{xy} \\ S'_{yx} & S'_{yy} \end{pmatrix} \cdot \begin{pmatrix} \frac{\partial T}{\partial x} \\ 0 \end{pmatrix} = \begin{pmatrix} S'_{xx} \cdot \frac{\partial T}{\partial x} \\ S'_{yx} \cdot \frac{\partial T}{\partial x} \end{pmatrix} \tag{S6}$$

so that

$$j_{yy} \propto \frac{1}{2}\Delta S \cdot \sin 2\theta \cdot \frac{\partial T}{\partial x}. \tag{S7}$$

Transverse thermoelectric effect requires that applying temperature gradient along x axis ($\frac{\partial T}{\partial x}$) will generate non-zero electric current density j_{yy}[3]. Clearly, transverse effect will be absent in those isotropic 2D materials with $\Delta S = 0$. Even for 2D material with in-plane anisotropy ($S_{xx} \neq S_{yy}$), transverse effect can only be obtained when temperature gradient is applied along the direction away from the principal axes, where $\sin 2\theta \neq 0$.

References

[1] G. She, X. Zhang, W. Shi, Y. Cai, N. Wang, P. Liu and D. Chen, *Cryst. Growth Des.*, 2008, **8**, 1789–1791.

[2] A. Togo, F. Oba and I. Tanaka, *Phys. Rev. B*, 2008, **78**, 134106.

[3] H. J. Goldsmid, *J. Electron. Mater.*, 2011, **40**, 1254–1259.